FIRST PRINCIPLES SIMULATION OF IRON-BASED INTERMETALLIC ALLOYS

Michael Widom[1], Libo Xie[1], Siddartha Naidu[1], Marek Mihalkovic[1,2], Don Nicholson[3] and Yang Wang[4]
[1]Department of Physics, Carnegie Mellon University, Pittsburgh, PA 15213
[2]Institute of Physics, Slovak Academy of Science, Bratislava, Slovakia
[3]Computational Physics Division, Oak Ridge National Laboratory, Oak Ridge, TN 37831
[4]Pittsburgh Supercomputer Center, Carnegie Mellon University, Pittsburgh, PA 15213

ABSTRACT

We carry out molecular dynamics simulations of Iron-based alloys using an ab-initio pseudopotential-based method to evaluate forces. Our focus is on glass-forming compounds including up to six different metal and metalloid elements, and calculations are carried out in both the equilibrium and supercooled liquid states. We extract structural information such as pair correlation functions and characteristic atomic clusters and also observe elemental diffusivities.

INTRODUCTION

Although no general and successful theory of bulk metallic glass formability exists as yet, we presume that among the relevant factors is the ability to nucleate and grow competing crystal structures. In a many-component alloy, phase segregation needed to grow thermodynamically stable intermetallic compounds is inhibited by two factors. A probabilistic effect known as the "confusion principle" inhibits phase separation because of the loss of entropy of mixing. Additionally, low diffusion constants of certain atomic species provide a kinetic effect. Implicit in this picture is the assumption that thermodynamically stable competing crystal structures exist only at compositions far from the amorphous alloy, and that the only metastable crystal structures near the amorphous alloy composition are structurally complex and difficult to grow.

We investigate these ideas in the context of Iron-based bulk metallic glass-forming alloys, using ab-initio total energy calculation and first-principles molecular dynamics to investigate the stability of competing crystalline phases, model the amorphous structure and evaluate diffusion constants in the supercooled liquid. Among our findings are:
1. Fe-B phase diagram (instability of interstitial and substitutional structures)
2. Strong links between atomic and amorphous structure and atomic size.
3. Atomic size effect on diffusivity.

Cohesive Energy

We investigate cohesive energies in the $Fe_{1-x}B_x$ binary alloy system. Our calculations are based on the Vienna Ab-initio Simulation Package (VASP, version 4.4.5 [1]). We use ultrasoft Vanderbilt type pseudopotentials as supplied by Kresse and Hafner [2]. As an exchange-correlation functional we use the Perdew-Wang (1991) Generalized Gradient Approximation and the Vosko-Wilk-Nusair interpolation [3]. All calculations are performed with collinear spin

polarization. Convergence studies were performed to optimize the plane wave energy cutoffs and k-point grids to achieve 1meV/atom accuracy on total energy differences. We found that VASP's medium precision setting sufficed. K-point grids of 8x8x8 up to 15x15x15 were employed for the crystalline structures. Liquid and amorphous structures containing 100 atoms in the simulation cell utilized the Gamma-point only.

x	Structure type	Pearson	Comments
0.000	W (BCC)	cI2	Known stable
0.200	Fe_4C	cP5	FCC with tetrahedral interstitials
0.200	Liquid		Simulated T=1500K liquid
0.200	Amorphous		Quenched (relaxed) from liquid
0.207	C_6Cr_{23}	cF116	Metastable in Fe-CB, distorted trigonal prisms
0.250	Fe3C	oP16	Known metastable, trigonal prisms
0.250	Ni_3P	tI32	Known metastable, distorted trigonal prisms
0.250	Fe_3Si	cF16	Ordered BCC solid solution
0.250	Fe_3C	hP8	HCP with octahedral interstitials
0.333	Al_2Cu	tI12	Known stable
0.500	BCr	oP8	Known stable
0.500	FeC	oC8	

Table 1. Structure types considered in cohesive energy calculations.

Up to Boron concentration of x=0.50 the equilibrium alloy phase diagram [4] contains stable phases for pure Fe (BCC), Fe_2B and FeB. Two metastable phases (of types oP16 and tI32) are reported. In addition to the known stable and metastable phases, we considered structures known in the Fe-C alloy system (metastable only). Our result (Fig. 1) reproduces the experimentally observed phase diagram, with stable phases appearing on the convex hull of the energy vs. composition plot. The known metastable phases at x=0.250 lie, respectively, about 10 and 20 meV/atom above the tie-line connecting pure BCC Iron to Fe_2B (shown here as horizontal).

The metastable Fe_3B phases are structurally complex, being based on edge-linked networks of capped trigonal prisms. In the case of oP16 these prisms are structurally perfect, while in tI32 they are distorted by a slight rotation of the triangular ends relative to each other. Similarly the metastable C6Cr23 structure, containing 116 atoms/unit cell, is based on metalloid atoms surrounded by distorted trigonal prisms. In contrast, the unstable (i.e. not observed) structure hP8 (Fe_3C) is HCP Iron with metalloid atoms at octahedral interstitial sites. Presumably, the larger size of B atoms relative to C (nominal atomic radii, respectively, 0.8Å and 0.7Å) would destabilize the crystal lattice when occupying the interstitial site. This effect is even more marked in the tetrahedral interstitial site of cP5 (Fe_4C). Likewise, the unstable cF16 (Fe_3Si) structure is an ordered solid solution of BCC iron with B substituted for Fe at alternate body centers. Presumably the small size of B relative to Fe (nominal atomic radius 1.2Å) destabilizes the BCC structure.

The cohesive energy plot suggests a mechanism for glass formation around the composition $Fe_{80}B_{20}$. Destabilization of simple crystal structures by atomic size contrast was suggested by Egami [5] as a mechanism for metallic glass formation. Our findings support this idea, with

simple crystal structures, which we imagine could easily nucleate and grow, being unstable as a result of atomic size effects. In order to for crystallization to occur, phase separation will be needed, at least to enable formation of the metastable Fe_3B structures. Rapid quenching permits neither the needed phase separation nor the nucleation of complex structure types. Their inhibition is aided by the low liquidus temperature arising from the nearby eutectic at $Fe_{83}B_{17}$.

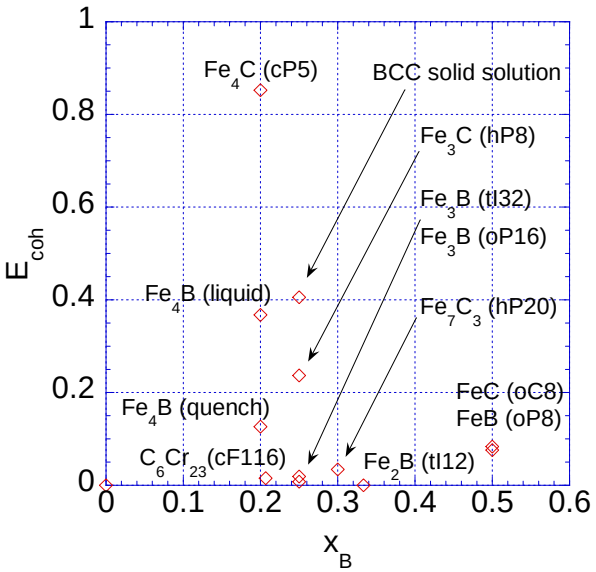

Figure 1. Cohesive energies of Fe-B alloys. See table for crystal types. See Molecular Dynamics section concerning liquid and quenched Fe4B structure.

Molecular Dynamics

To further probe the above proposed glass formation mechanism we perform molecular dynamics simulations of pure Fe, Fe-B and Fe-Zr-B. Our calculations again use VASP. Liquid state calculations employ systems of 100 atoms in an orthorhombic cell, typically with dimensions a=10Å, b=11Å, c=10-12Å, where we adjust c to fix the desired atomic volume. We again perform spin-polarized calculations to mimic the role of localized magnetic moments which exist even in the liquid state. For molecular dynamics runs we used a time step of 2 fs in a Verlet algorithm using a Nose thermostat in the canonical ensemble.

Figure 2(a) shows the simulated pair correlation function g(r) of liquid Fe at its experimental melting point (T=1833K) and number density (n=0.0756/Å^3), compared with the experimental data [6]. Although the simulation agrees qualitatively with experiment, a clear disagreement is found in the position of the peak. Experimentally the peak position is around 2.56Å, while the simulated position is around 2.46Å. This short Fe-Fe bond length remains in the simulation regardless of the calculational precision, number of k-points, number of atoms, atomic volume, etc. We believe it is an intrinsic (and erroneous) property of the pseudopotential

being used. Our simulation shows more structure at long lengths than the experiment. A more recent experimental study [7] is closer to our simulation at long lengths but with a similar discrepancy in the near neighbor bond length. Our calculations obtain a magnetic moment of

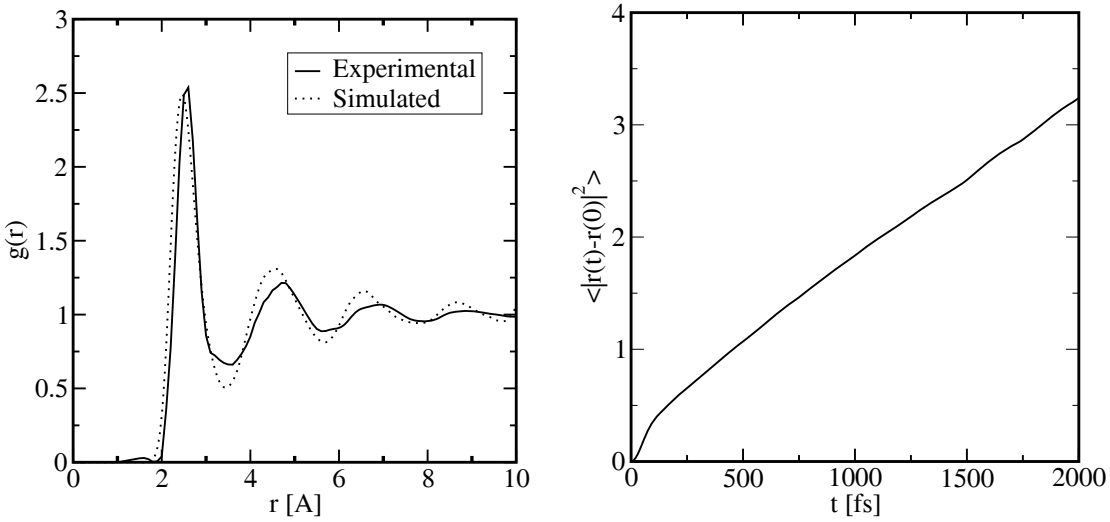

Figure 2 (a) Experimental and simulated pair correlation functions for pure liquid Fe at melting temperature T_m=1833K. **(b)** Mean square atomic displacement during MD simulation. Total run time was 2.5 ps.

We monitor the time-correlation function $<|r(t)-r(0)|^2>$ during the run (Fig. 2(b)). At early times it grows quadratically (like $(3k_BT/M)t^2$) reflecting the ballistic motion of individual atoms. In a single 2fs time step of our molecular dynamics simulation the RMS atomic displacement is 0.02A, about 1% of the typical interatomic distance. At later times this crosses over to a nearly linear behavior, growing like 6Dt as t increases. From the slope of the linear portion (about 1.4 $Å^2$/ns) we estimate the diffusion coefficient D~2.3 x 10^{-9} m^2/s. Experimental values of the diffusion coefficient are not known, though an estimate of 4 x 10^{-9} m^2/s based on an equivalent hard sphere model is sometimes quoted [9].

Having thus evaluated the ability to reproduce known equilibrium liquid structure, we now address the simulation of Fe-B and FeZrB. Consider the effect of alloying on the effective Fe atomic size and diffusion constant. Examining first the FeFe correlations (Fig. 3), we find two effects with B and Zr alloying. The position of the FeFe peak shifts to the right (from 2.48 to 2.52Å) when alloying with B, then shifts back to the left upon alloying with Zr. We suspect this reflects the charge transfer between Fe and the alloying elements B (greater electronegativity) and Zr (lesser electronegativity). Additionally, Zr tends to quench the magnetic moment of the Fe atoms, leading again to reduced bond length. The other structural effect is a reduction in the amplitude of long-range oscillations. The pure Fe liquid is highly structured at long lengths while the FeB and especially FeZrB alloy lose their correlation more rapidly.

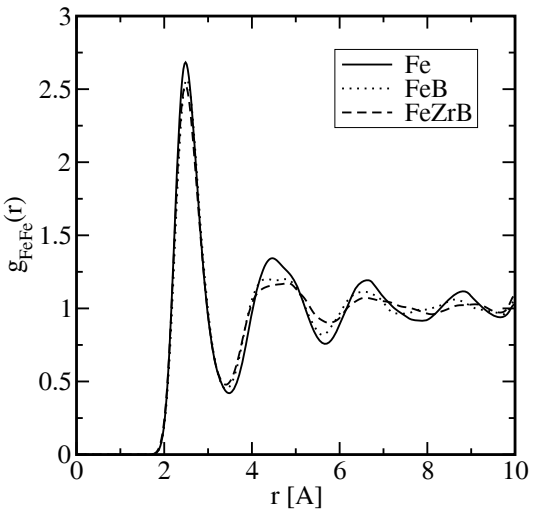

Figure 3 FeFe pair correlation functions calculated for pure Fe, FeB and FeZrB liquids at T=1500K.

Unlike the case of pure liquid Fe, there is little experimental guidance for the atomic volumes of liquid Fe-based alloys, and we are unable to calculate this from first principles because VASP version 4.4.5 lacks the capability to perform constant pressure molecular dynamics. To obtain an appropriate atomic volume for our high temperature simulations we first performed static relaxations of trial amorphous structures to get the atomic volume in the quenched glassy state, then we increased these volumes by 7% to estimate the atomic in the liquid state at T=1500K. The value of 7% was chosen because it is slightly less than the reported volume ratio of 8% between the atomic volumes of T=1600K liquid and amorphous $Fe_{75}B_{25}$ alloys [10].

In terms of diffusion (see Fig. 4(a)), alloying with B has little effect on Fe diffusion rates. On the other hand, alloying with Zr leads to significantly enhanced Fe diffusion. This could be due in part to the reduced Fe effective size (or effective charge) connected with electronegativity differences and resulting charge transfer. Further study of this effect will be necessary. Even more dramatic are the relative diffusion rates of the different atomic species (Fig. 4(b)). Clearly atomic size plays a large role in setting the diffusion constant. According to the Stokes-Einstein relation, the diffusion constant of a hard sphere of radius R in a fluid of viscosity η is $D=k_BT/6\pi\eta R$. However, the apparent diffusivity ratios of B:Fe:Zr (roughly 2.2:1.0:0.4 in units of 10^{-9} m^2/s, taken from Fig. 4(b)) show far greater variation than the nominal size ratios (roughly 0.8:1.2:1.6 in units of Å). Qualitatively, we see the small atoms diffuse quickly and the large atoms slowly, but quantitatively the Stokes-Einstein relation does not apply. A more detailed theory of diffusion is needed, taking into account the actual diffusion pathways, attempt frequencies and caging phenomena.

Slow diffusion of Zr atoms probably plays a crucial role in glass formability in Fe-Zr-B alloys. Even at a concentration as low as 10% the large Zr atoms can destabilize the metastable Fe_3B structures. By preventing phase separation into Zr-free regions where the Fe_3B phases can nucleate, the Zr atoms inhibit crystallization. However, it is likely that Zr atoms can be incorporated into the C_6Cr_{23} structure, which our cohesive energy study has shown to be nearly stable. Hence we believe that a limiting factor in glass formation in Fe-Zr-B alloys may be the difficulty of nucleation and growth of the highly complex cF116 structure.

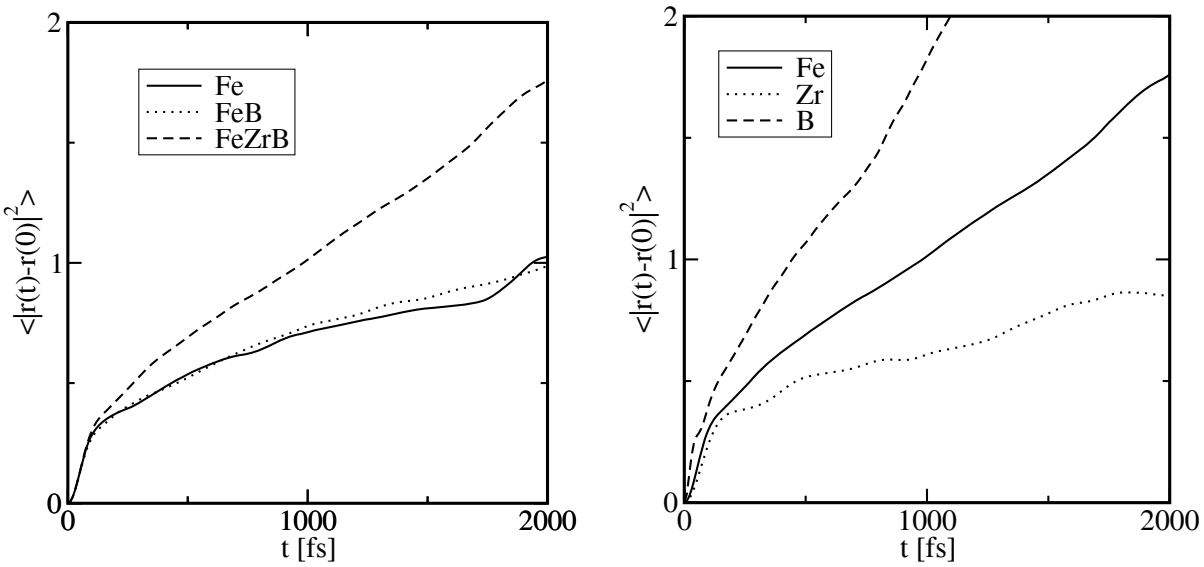

Figure 4 (a) Fe diffusion for pure Fe, FeB and FeZrB liquids. (b) Fe, Zr and B diffusion in liquid FeZrB. All data from T=1500K simulations. All simulations of 2.5 ps or longer.

ACKNOWLEDGEMENTS

This research was supported by DARPA/ONR Grant N00014-01-1-0961. We wish to acknowledge useful discussions with Joe Poon, Despina Louca, Gary Shiflet and Takeshi Egami.

REFERENCES

1. G. Kresse and J. Hafner, Phys. Rev. B 47, RC558 (1993); G. Kresse, PhD Thesis, Technische Universität Wien 1993; G. Kresse and J. Furthmüller, *Comput. Mat. Sci*. **6**, (1996) 15-50; G. Kresse and J. Furthmüller, *Phys. Rev. B* **54**, 11169 (1996).
2. D. Vanderbilt, Phys. Rev. B41 7892 (1990); G. Kresse and J. Hafner, *J. Phys.: Condens. Matter* **6**,(1994) 8245.
3. S. H. Vosko, L. Wilk and M. Nusair, *Can. J. Phys.* **58**, (1980) 1200
4. T.B. Massalski, H. Okamoto, P.R. Subramanian and L. Kacprzak, eds. *Binary Alloy Phase Diagrams* (ASM, 1990) p. 480-3
5. T. Egami and Y. Waseda, *J. Noncryst. Solids* **64** (1984) 113-34
6. Y. Waseda, *The Structure of Non-crystalline materials: liquids and amorphous solids* (McGraw-Hill, 1980)
7. T. Schenk, D. Holland-Moritz, V. Simonet, R. Bellissent and D.M. Herlach, *Phys. Rev. Lett.* **89** (2002) 075507
8. W. Matz, B. Kunsch and E. Wieser, *Phys Stat Sol A* **76** (1983) K1 7-20
9. P. Protopapas, H.C. Andersen and N.A.D. Parlee, *J. Chem. Phys*. **59** (1973) 15-25
10. For $Fe_{75}B_{25}$ amorphous and liquid atomic volumes, see Y. Waseda and H.S. Chen, *Phys. Stat. Sol*. **A49** (1978) 387-392; N. Mattern, W. Matz and H. Hermann, *Z. Nat*. **A43** (1988) 177-180